Mass of Dust in the Martian Atmosphere

TERRY Z. MARTIN

Jet Propulsion ***Laboratory,***

California Institute @Technology,

Pasadena CA 91109

Feb. 241994

Manuscript pages: 6

Figures: 2

Tables: “ 1

Suggested running head: Martian atmospheric dust content

Direct correspondence to:

Terry Z. Martin
Mail stop 169-237
Jet Propulsion Laboratory
4800 Oak Grove Dr.
Pasadena CA 91109
(818) 354-2178
FAX: (818) 393-4619

Abstract

Estimates of the mass of dust suspended in the Martian atmosphere are derived from global and regional 9 μm opacity maps produced from Viking Infrared Thermal Mapper data. During the peak of the 1977b storm, a total dust mass of approximately 10^{15} gm was suspended, equivalent to 10^{-3} gm/cm^2, or a layer 4 μm thick. During a local dust storm near Solis Planum at L_s 227°, approximately 3.56 x 10^{13} gm of dust were lofted, equal to about an 18 μm layer in that vicinity.

INTRODUCTION

The amount of dust present in the Martian atmosphere is of interest for several reasons. From a radiative point of view, dust strongly affects the dynamical state of the atmosphere, as well as the amount of sunlight reaching the surface. For that purpose, the amount of dust is adequately characterized by the optical depth, or opacity. Another viewpoint is that of surficial geology: how much dust can be deposited or removed by storms over a given period of time? Finally, the amount of dust is an engineering parameter of interest to those designing solar arrays or optical instruments for use on the surface. For the latter applications, the mass of dust, or the thickness of a deposited layer, is the relevant quantity.

A set of global opacity maps for Mars was recently published [*Martin*, 1993]. They present the 9 μm (silicate band) optical depth of dust as a function of latitude, longitude, and seasonal parameter L_S (areocentric solar longitude). In this paper we endeavor to convert those maps to estimates of global dust content, expressed in grams. This quantity may then be expressed as a mass per unit area or a layer of some thickness, for a given density. A typical local dust storm can be treated in similar fashion to estimate the dust raised by such events.

ASSUMPTIONS

In order to convert the total path opacity values computed by Martin to precipitable dust amounts, several assumptions are necessary. Some of these relate to the nature of the dust, and others relate to the lack of truly global coverage by the Viking observations.

We employ here an expression used by Pollack *et al [1979]* to do a similar conversion for Viking Lander opacity values:

$$m = \frac{2}{3}\bar{r}\rho\tau \qquad \text{gm/cm}^2\text{, where} \qquad (1)$$

$\bar{r}$ is the mean particle radius, p is particle density, and τ is optical depth in the visual region.

In order to compute the mass over an area of the planet, we simply take the mass corresponding to the opacity of an individual latitude/longitude bin of the opacity map, multiply by the area of that bin, and sum over bins.

$$M = \frac{1}{A}\sum_i a_i m_i \qquad \text{gm, where} \qquad (2)$$

A is the relevant area of the planet.

Since the expression employed by Pollack *et al* was derived for visual region opacity, there is a need to introduce a factor relating the visual to 9 μm opacities. According to Martin [1986], this factor is approximately 2, with the infrared values being lower.

An additional important assumption is that the opacity behavior of the parts of the planet that are not sampled is the same as for the covered fraction. Those opacity maps covering a larger fraction of the planet will give a correspondingly better estimate of the total dust mass. The mass for the sampled area is divided by the fraction covered to correct for the undersarnpling:

$$M_{total} = M_{sampled} \,/ f \quad . \qquad (3)$$

We treat first the mass of dust raised by the major storms seen by Viking, referred to as 1977a and 1977b. For each of the 5° L_S opacity maps, we create the total mass of dust corresponding to the populated latitude/longitude bins. We also derive the fraction of the planet's area represented by these bins. Making the undersampling correction, we estimate the total dust mass represented by the measured opacities (Table 1). The result of applying this process to the opacity map series is a profile of dust content (Fig. 1) highly reminiscent of other opacity histories that have been developed for the Viking era [Thorpe, 1979,1 981; Zurek, 1981; Martin, 1986; Colburn et al, 1989]. In both Martian years covered, there is an increase in atmospheric dust loading beginning near L_S 140°; this increase amounted to about a fivefold change during the first year, but only about a factor of three in the second. For the first year, a series of major storm events contributed to the overall dust content, leading to a peak loading near the time of southern summer solstice (Ls 270°). It is noteworthy that the process of correcting for partial sampling does not seem to have introduced substantial noise into the curve of dust mass versus time, at least where more than about 10% of the planet is covered. Note that the decay phases of the two major storms 1977a and b are monotonic, and that the relatively clear period following the storms is quite smooth.

The maximum dust content during the 1977b storm amounted to about 1.2 x 10^{15} gm; this corresponds to about 10^{-3} gm/cm^2, or a layer 4 μm thick. This is half the amount estimated by Pollack *et al [1979]* to be deposited over a Martian year, based upon his analysis of the same storm period from Viking Lander opacity values. If the depositional stage of this storm season was quiescent, then it can be assumed that about 10^{-3} gm/cm^2 of dust was evenly deposited over most of the planet. On a smooth surface, this amount is more than adequate to obscure underlying dark material and change the apparent albedo; such behavior is consistent with observations of albedo change following major storms [Greeley et *al*, 1992],

LOCAL STORMS

A number of localized dust storm events were seen by Viking, both in the imaging data and by the IR Thermal Mapper. We examine here one particularly well-known case, that of a storm seen at L_s 227° by both instruments, south of Vanes Marineris [Briggs et al, 1979; Peterfreund and Kieffer, 1979; Hunt et al, 1980]. Opacity maps of this storm were generated using the same algorithm employed for the global mapping, but applied to three successive individual IRTM observational sequences, essentially snapshots in time (Fig. 2). For this purpose, in order to retain maximum spatial resolution, individual 7 μm samples were paired with nearest-neighbor 9 μm and 15 μm samples, and the location of the derived opacity assigned to the average location of the 7 and 9 μm samples. See Martin [1986] for a discussion of the approach to use of the IRTM data for opacity derivation.

The central region of the storm is taken to be a rectangular area 4 pixels in latitude by *6* in longitude (12 by 180), which is 7.1 x 105 km2 at latitude -20°. These 24 pixels contribute a total opacity in the central frame of Fig. 2 that is 888 DN above the background value of 69 DN, where the maximum value of 255 corresponds to a 9 μm opacity of 2.0. Using the formula (2) above, this total implies a dust mass of 3.56 x 10^{13} gm above that due to the background dust loading, or an enhancement of 50,000 kg/km^2. This is the equivalent of an 18 μm layer, or about four times more dust than the global value calculated above for the peak of the 1977b storm.

ANALYSIS

The dust abundances derived above can be used in a variety of ways. It must be emphasized that the dust amounts calculated indicate a transient situation, and that the origin and fate of this dust are not known. For the local storm particularly, the dust raised may not have been derived from the same area used for the sampling, and it may not be deposited in that area either. If local storms become inactive at night, it is likely that some large-particle fraction of the dust is deposited diurnally and locally, while a smaller-particle component remains aloft and becomes more distributed areally with time.

It is well established that the occurrence of major dust storms on Mars is not a reliable yearly event [Zurek and Martin, 1993]; only a few truly global dust storms have been seen during the century that Mars has been regularly monitored telescopically. For this reason, it is misleading to assign the dust masses derived above to typical annual behavior, It is also very difficult to derive a useful average annual deposition rate. The Martian atmosphere since Viking has been found to be substantially clearer [Clancy, Muhleman, and Berge, 1990]. It may be that most of the dust redistribution occurs only during relatively infrequent periods of activity, analogous to the modification of terrestrial surfaces by rare catastrophic flood events.

It should also be noted that the dust masses computed here depend directly on the derived opacities, and as such are dependent on whatever errors may arise in that calculation. For example, in the case of a very thick dust cloud, the 7 μm IR brightness temperature may not adequately represent surface conditions. In such a case, the opacity would be a lower limit, and the same applies to dust mass.

Acknowledgments. The research described in this paper was carried out by the Jet Propulsion Laboratory, California Institute of Technology, under a contract with the National Aeronautics and Space Administration. This work was supported by the Mars Surface and Atmosphere Through Time (MSATT) program.

REFERENCES

Briggs, G.A., W.A. Baum, and J. Barnes, Viking Orbiter imaging observations of dust in the martian atmosphere, *J. Geophys. Res.,* 84, 2795, 1979.

Clancy, R,T., D.O. Muhleman and G.L. Berge, *J. Geopys. Res.,* 95, 14,543-14,554, 1990.

Colburn, D. S., J. B. Pollack, and, R. M. Haberle, Diurnal variations in optical depth at Mars, *Icarus,* 79, 159, 1989.

Greeley, R., N. Lancaster, S. Lee, and P. Thomas, Martian aeolian processes, sediments, and features, in Mars, edited by Kieffer, Jakosky, Snyder, and Matthews, Univ. of Arizona press, 1992.

Hunt, G, E., E.A. Mitchell, and A.R. Peterfreund, The opacity of some local Martian dust storms observed by the Viking IRTM, *Icarus,* 41,389, 1980.

Martin, T.Z., Thermal infrared opacity of the Mars atmosphere, *Icarus,* 66,2, 1986,

Martin, T.Z. and M.I. Richardson, New dust opacity mapping from Viking Infrared Thermal Mapper data, *J. Geophys. Res.* 98, 10941-10949, 1993.

Peterfreund, A. R., and Kieffer, H. H., Thermal infrared properties of the Martian atmosphere. 3. Local dust storms. *J. Geophys. Res.* 84, 2853-2863, 1979.

Pollack, J. B., D. Colburn, F.M. Flasar, R. Kahn, C. Carlston, and D. Pidek, Properties and effects of dust particles suspended in the Martian atmosphere, *J. Geophys. Res.,* 84, 2929, 1979.

Thorpe, T.E., A history of Mars atmospheric opacity in the southern hemisphere during the Viking extended mission. J, *Geophys. Res.* 84,6663-6683, 1979.

Thorpe, T.E., Mars atmospheric opacity effects observed in the northern hemisphere by Viking Orbiter imaging. *J. Geophys. Res.* 86, 11419-11429, 1981.

Zurek, R.W., Inference of dust opacities for the 1977 Martian great dust storms from Viking Lander 1 pressure data. *Icarus* 45,202-215, 1981,

Zurek, R.W., and L.J. Martin, Interannual variability of planet-encircling dust storms on Mars, *J. Geophys. Res.,* 98, 3247, 1993.

FIGURE captions

Fig. 1. (Points) Dust mass in the Martian atmosphere versus seasonal parameter L_s for the period from 1976-78; scale at left. (Dashed) Fraction of the region between ±60° latitude sampled in each opacity map; scale at right. Note that poor areal coverage at the beginning and end of the Viking mission may skew the derived global masses.

Fig. 2. Opacity maps (9 μm) of local dust storm observed on March 241977 (L_s 2270). (Top) 0017 hours UTC; (middle) 0147; (bottom) 0347.

TABLE 1. Dust Mass Calculations

F_{total} = Fraction of area of planet covered
F_{60} = Fraction of area between ±60° latitude covered

L_S (start)	F_{total} - -	Total mass	F_{60}	Mass ±60°	Corrected mass
80	0.00	1.37E+12	0.00	1.25E+12	2.72E+14
85	0.06	2.20E+13	0.06	1.89E+13	3.06E+14
90	0.00	4.99E+11	0.00	3.49E+11	1.33E+14
95	0.02	2.81E+12	0.02	2.40E+12	1.01E+14
100	0.05	1.07E+13	0.05	9.10E+12	1.80E+14
105	0.06	1.23E+13	0.04	8.92E+12	2.00E+14
110	0.11	6.79E+12	0.10	4.56E+12	4.63E+13
115	0.05	2.44E+12	0.05	2.02E+12	4.09E+13
120	0.38	2.31E+13	0.41	2.04E+13	5.03E+13
125	0.21	1.13E+13	0.22	9.95E+12	4.53E+13
130	0.11	6.08E+12	0.11	4.41E+12	4.17E+13
135	0.13	9.80E+12	0.13	8.78E+12	6.68E+13
140	0.11	1.21E+13	0.09	8.78E+12	9.58E+13
145	0.22	4.05E+13	0.17	2.72E+13	1.64E+14
170	0.27	9.57E+13	0.27	9.02E+13	3.33E+14
175	0.32	1.11E+14	0.37	1.17E+14	3.17E+14
180	0.36	1.01E+14	0.39	1.02E+14	2.62E+14
185	0.40	1.04E+14	0.47	1.09E+14	2.29E+14
190	0.46	1.64E+14	0.52	1.59E+14	3.06E+14
195	0.55	1.45E+14	0.65	1.50E+14	2.32E+14
200	0.36	1.12E+14	0.44	1.20E+14	2.71E+14
205	0.24	1.72E+14	0.28	1.67E+14	5.94E+14
210	0.21	1.95E+14	0.24	1.99E+14	8.18E+14
215	0.57	5.42E+14	0.66	5.35E+14	8.09E+14
220	0.47	4.12E+14	0.54	4.01E+14	7.49E+14
225	0.46	3.74E+14	0.54	3.84E+14	7.07E+14
230	0.33	2.58E+14	0.38	2.60E+14	6.77E+14
235	0.32	2.08E+14	0.35	1.97E+14	5.66E+14
240	0.47	2.79E+14	0.52	2.68E+14	5.16E+14
245	0.49	2.59E+14	0.53	2.42E+14	4.58E+14
250	0.43	2.01E+14	0.47	1.85E+14	3.96E+14
255	0.59	2.65E+14	0.67	2.56E+14	3.84E+14
260	0.63	2.49E+14	0.69	2.38E+14	3.42E+14
265	0.37	1.35E+14	0.42	1.30E+14	3.10E+14
270	0.29	1.46E+14	0.35	1.57E+14	4.50E+14
275	0.38	4.28E+14	0.45	4.49E+14	9.88E+14
280	0.39	5.12E+14	0.47	5.42E+14	1.14E+15
285	0.23	3.12E+14	0.28	3.36E+14	1.21E+15
290	0.22	2.79E+14	0.27	2.96E+14	1.09E+15
295	0.40	4.97E+14	0.46	5.03E+14	1.09E+15
300	0.42	4.46E+14	0.49	4.64E+14	9.39E+14
305	0.33	3.14E+14	0.38	3.13E+14	8.34E+14
310	0.54	3.76E+14	0.63	3.83E+14	6.11E+14
315	0.34	1.97E+14	0.39	1.92E+14	4.97E+14
320	0.42	2.01E+14	0.50	2.04E+14	4.08E+14
325	0.36	1.39E+14	0.41	1.35E+14	3.30E+14
330	0.42	1.42E+14	0.49	1.37E+14	2.80E+14
335	0.46	1.44E+14	0.52	1.36E+14	2.61E+14
340	0.64	1.85E+14	0.72	1.67E+14	2.32E+14
345	0.59	1.21E+14	0.68	1.16E+14	1.69E+14
350	0.56	1.10E+14	0.65	1.02E+14	1.58E+14

355	0.57	1.07E+14	0.63	9.57E+13	1.51E+14
360	0.46	6.98E+13	0.53	6.69E+13	1 .25E+14
5	0.56	7.05E+13	0.60	6.17E+13	1.03E+14
10	0.48	5.68E+13	0.48	4.71E+13	9.72E+13
15	0.35	4.57E+13	0.35	3.71E+13	1.06E+14
20	0.67	7.09E+13	0.66	5.49E+13	8.33E+13
25	0.60	6.12E+13	0.58	4.44E+13	7.58E+13
30	0.60	7.53E+13	0.57	5.66E+13	9.92E+13
35	0:60	6.12E+13	0.55	4.34E+13	7.84E+13
40	0.53	5.00E+13	0.47	3.60E+13	7.57E+13
45	0.58	5.65E+13	0.53	4.02E+13	7.63E+13
50	0.42	3.88E+13	0.35	2.34E+13	6.70E+13
55	0.41	4.01E+13	0.33	2.41E+13	7.35E+13
60	0.35	3.28E+13	0.26	1.77E+13	6.80E+13
65	0.36	3.56E+13	0.26	2.07E+13	8.06E+13
70	0.39	3.57E+13	0.28	1.81E+13	6.41E+13
75	0.30	2.67E+13	0.20	1.26E+13	6.17E+13
80	0.24	2.10E+13	0.13	8.12E+12	6.13E+13
85	0.21	2.23E+13	0.12	5.86E+12	4.74E+13
90	0.25	2.82E+13	0016	1.54E+13	9.37E+13
95	0.32	3.17E+13	0.22	1.65E+13	7.47E+13
100	0.22	1.88E+13	0.13	8.63E+12	6.48E+13
105	0.22	1.71E+13	0.13	7.14E+12	5.54E+13
110	0.24	1.93E+13	0.16	1.00E+13	6.36E+13
115	0.19	1.03E+13	0.12	4.91E+12	4.01E+13
120	0.19	1.40E+13	0.11	5.63E+12	5.12E+13
125	0.20	1.50E+13	0.13	7.64E+12	5.85E+13
130	0.20	1.10E+13	0.13	5.58E+12	4.20E+13
135	0.22	1.19E+13	0.15	6.11E+12	4.15E+13
140	0.21	2.17E+13	0.15	1.19E+13	8.12E+13
145	0.20	2.56E+13	0.15	1.60E+13	1.10E+14
150	0.24	4.47E+13	0.19	3.09E+13	1.63E+14
155	0.22	3.36E+13	0.17	2.24E+13	1.33E+14
160	0.22	5.33E+13	0.18	3.98E+13	2.18E+14
165	0.24	4.78E+13	0.21	3.65E+13	1.77E+14
170	0.21	3.26E+13	0.19	2.58E+13	1.40E+14
175	0.16	2.25E+13	0.15	1.82E+13	1.20E+14
180	0.15	2.70E+13	0.16	2.46E+13	1.57E+14
185	0.04	8.87E+12	0.04	8.12E+12	2.13E+14
190	0.06	1.58E+13	0.07	1.38E+13	2.08E+14
195	0.03	7.65E+12	0.04	7.75E+12	2.09E+14
200	O*03	6.75E+12	0.04	6.82E+12	1.84E+14
205	0 ."01	1.81E+12	0.01	2.15E+12	1.89E+14
210	0.01	2.35E+12	0.02	2.85E+12	1.78E+14
215	0.01	2.37E+12	0.02	2.84E+12	1.86E+14
220	0.01	2.50E+12	0.02	2.96E+12	1.77E+14
225	0.02	4.21E+12	0.02	4.98E+12	2.01E+14
230	0.02	4.80E+12	0.03	5.71E+12	2.25E+14

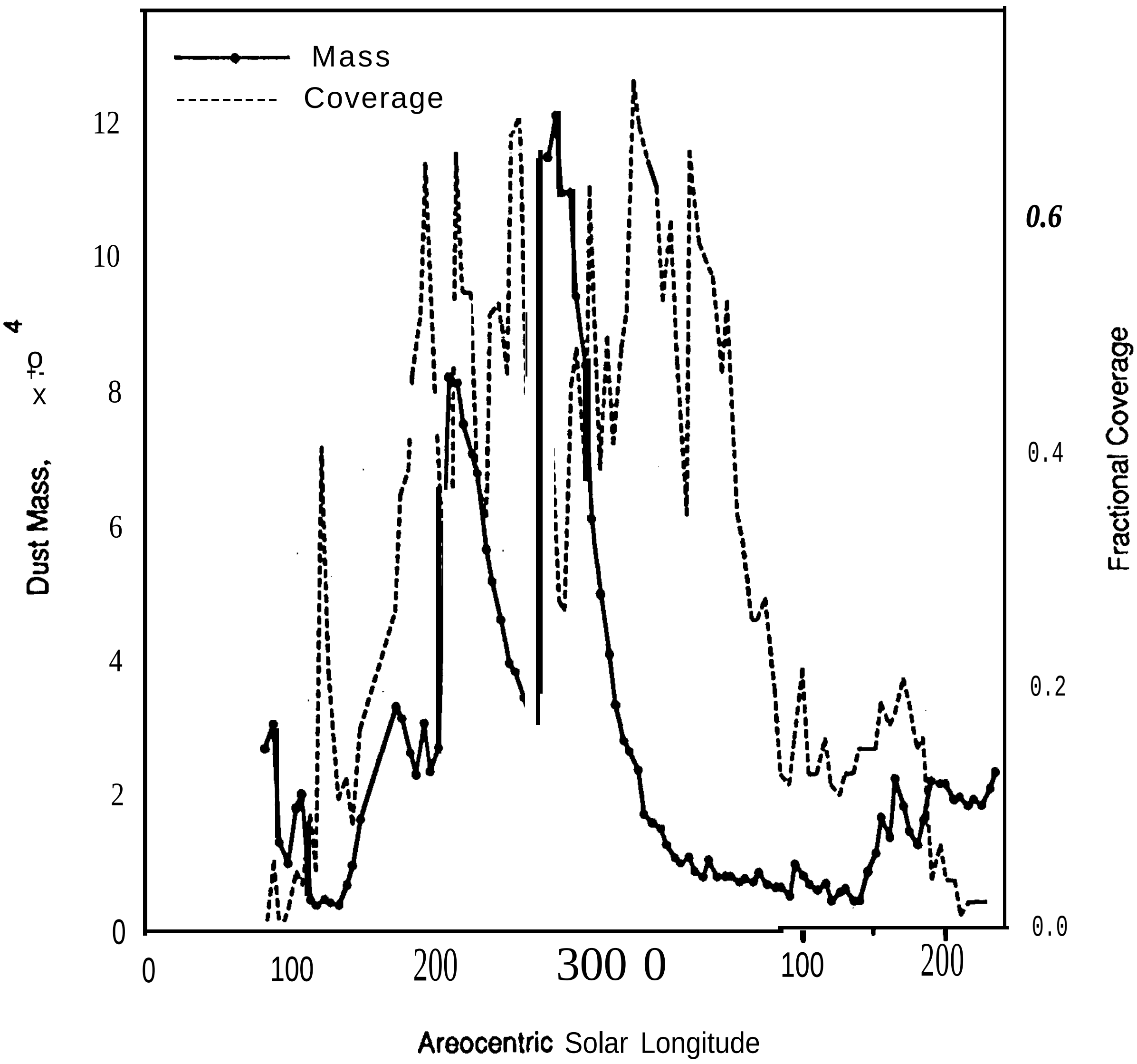

Mass
Coverage
Dust Mass, x 10^4
Fractional Coverage
0
2
4
6
8
10
12
0.0
0.2
0.4
0.6
0
100
200
300 0
100
200
Areocentric Solar Longitude

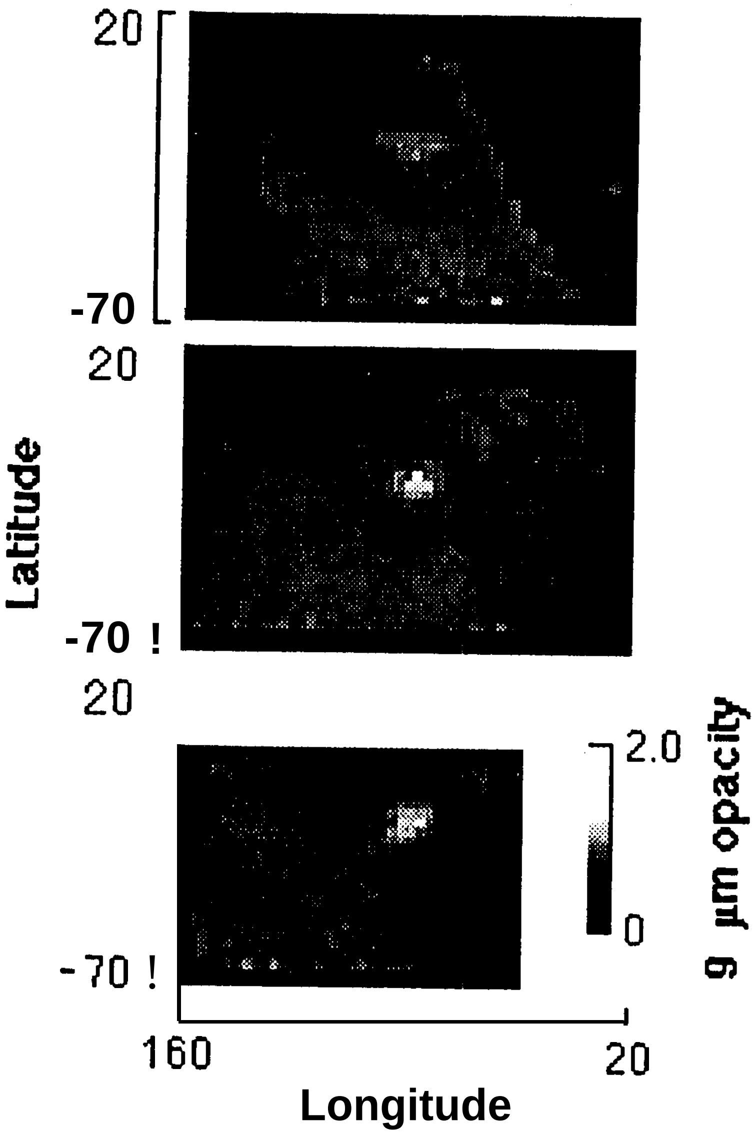

20
-70
20
-70 !
20
-70 !
Latitude
2.0
0
9 μm opacity
160
20
Longitude